Linear stability analysis of turbulent flows over dense filament canopies

Akshath Sharma, Garazi Gómez-de-Segura & Ricardo García-Mayoral

Department of Engineering
University of Cambridge
Cambridge, CB21PZ, UK
as2527@cam.ac.uk, gg406@cam.ac.uk & r.gmayoral@cam.ac.uk

ABSTRACT

The aim of this work is to study the effect of the variation in canopy parameters on the Kelvin-Helmholtz-like instabilities triggered over them. The appearance of these instabilities over filament canopies has been widely studied, but the present work seeks to explore whether the instability can be manipulated by changing canopy properties. To this effect, a parametric study using linear stability analysis is conducted. For the analyses, the canopy is modelled using two methods. The first models the canopy as a permeable substrate. The second accounts for the canopy through drag forces acting on the flow within it. Some effects of canopy dynamics, namely the average bending of the canopy elements and the dynamic clustering of the canopy are also individually studied. Using the porous medium analogy it is shown for rigid canopies that the onset of the instabilities is governed by the geometric mean of the streamwise and wall-normal permeabilities $\left(\sqrt{K_x^+ K_y^+}\right)$. The drag model exhibits an additional feature missed by the porous model i.e. an optimum value of drag coefficient at which the amplification of the instability is maximum. It is also observed that the clustering of filaments caused by the waving of the canopy can significantly increase the amplification of the instability, and has a greater impact than the mean filament bending.

INTRODUCTION

Existing studies regarding canopy flows, summarised in Finnigan (2000) and Nepf (2012), attribute the coherent waving seen in canopies, termed '*honami*' (Inoue, 1955), to a Kelvin-Helmholtz-like instability originating at the canopy top as shown in the schematic in Fig. 1. However, most of these studies focus on vegetation canopies. Consequently, the set of different canopy parameters studied has been restricted. An extensive examination of these parameters would find use in designing of canopy-based devices for energy harvesting, heat exchange and flow control, where the optimum layout could be very different to those found in nature. As a preliminary step in this direction, to sweep over a large number of canopy parameters we perform a linear stability analysis on the turbulent mean flow overlying filament canopies. Such analysis has been used by several authors (Raupach *et al.*, 1996; Jiménez *et al.*, 2001; Py *et al.*, 2006; White & Nepf, 2007; Ghisalberti & Nepf, 2009; García-Mayoral & Jiménez, 2011; Dupont *et al.*, 2010; Singh *et al.*, 2016; Zampogna *et al.*, 2016; Luminari *et al.*, 2016) to capture the spanwise-homogeneous Kelvin-Helmholtz-like instabilities which are characteristic of these flows. The applicability of linear stability analysis on a turbulent mean flow to predict strong convective instabilities, such as Kelvin-Helmholtz, has been demonstrated by Beneddine *et al.* (2016). To facilitate the parametric study of canopy layouts we model the flow within the canopy using two approaches. The first of these assumes the canopy to be analogous to a permeable substrate with the streamwise permeability smaller than the wall-normal one ($K_x/K_y < 1$). A similar analysis was carried out by Abderrahaman-Elena & Garcia-Mayoral (2015), who used Darcy's equation as a model for the flow within the permeable

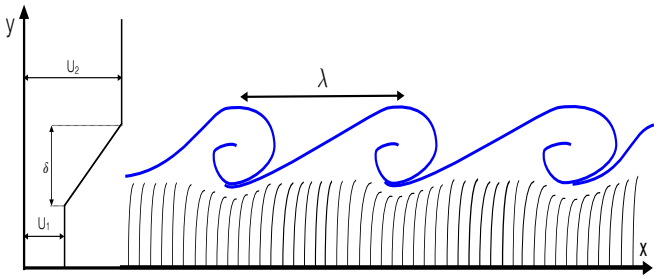

Figure 1: Schematic of a Kelvin-Helmholtz-like instability over a filament canopy. λ represents the wavelength of the instability, δ is the shear layer thickness at the canopy top.

substrate. To account for macroscale diffusive effects within the canopy, we also include the Brinkman term (Brinkman, 1949) in the equations. This is similar to the homogenisation approach used by Zampogna & Bottaro (2016) and Lacis & Bagheri (2017) to resolve the flow within the canopy. These studies also use Darcy's equations to model flow within the canopy. The use of Darcy's equations, which are first order, required them to use special interface conditions to connect the flow in the channel to that within the canopy (Ochoa-Tapia & Whitaker, 1995; Beavers & Joseph, 1967). Zampogna *et al.* (2016) and Luminari *et al.* (2016) subsequently performed stability analyses around the mean velocity profiles obtained using this method and report good agreement between their predictions of the most unstable wavelength and corresponding experimental observations. The second approach used in the present study, which models the effect of canopies on the flow as a drag force in the momentum equations is more conventional and has been used by Singh *et al.* (2016), Ghisalberti & Nepf (2009) and White & Nepf (2007) to study stiff canopies, and by Dupont *et al.* (2010) and Py *et al.* (2006) for oscillating canopies. Py *et al.* (2006) were the first to study the effect of canopy motion on instabilities using a linear stability analysis on a piecewise linear velocity profile. They coupled the filament motion to the flow around them using a fluctuating drag term- $K(u - dq/dt)^2$, where K is the drag coefficient, u is the flow velocity and q is the deflection of the filament, therefore taking into consideration the effect of filament oscillation. This study predicted the lock in of the flow instability with the frequency of filament oscillation for certain filament properties. Dupont *et al.* (2010) extended the analysis by performing an LES of the flow over waving filaments using the same coupling, but did not find the lock in effect to be significant for their case. However, these studies did not account for another effect that the waving of filaments cause, i.e. the clustering of filaments. Here we model this effect by letting the drag coefficient vary with the change in canopy density due to the waving. In addition, our models take into consideration the effect of filament orientation and reconfiguration under a mean flow, as well as the obstruction of the wall-normal velocity by the canopy.

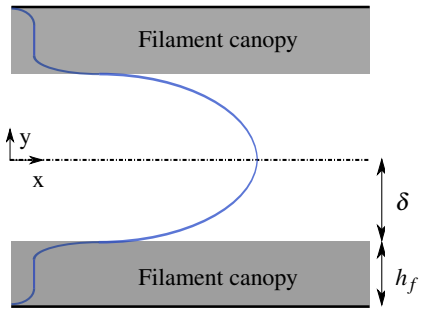

Figure 2: Schematic representation of the channel and streamwise velocity profile.

We consider symmetric channels as shown in Fig. 2, with a constant half-height δ with different canopy parameters. For the permeable substrate model, the parameters are the canopy height, h_f, and the streamwise and wall-normal permeabilities, K_x and K_y. For the drag model, the parameters are h_f and the drag coefficients, C_x and C_y, which essentially play the same roles as K_x^{-1} and K_y^{-1}.

METHODOLOGY

Porous medium analogy

Within the canopy, the flow is assumed to be Stokesian and is modelled using Brinkman's equation

$$\nu\nabla^2\vec{u} - \nu\mathbf{K^{-1}}\vec{u} - \nabla p = 0 \tag{1}$$

where ν is the kinematic viscosity of the fluid, $\vec{u}$ is the velocity vector and p is the pressure. The latter two terms of the equation represent the volume average of Stokes flow between the densely packed filaments. The first term captures the macroscopic diffusion occurring at scales larger than that of the volume averaging. The inverse permeability tensor $\mathbf{K^{-1}}$ depends on the local inclination of the canopy with respect to the vertical θ

$$\mathbf{K^{-1}} = \begin{bmatrix} \frac{\cos^2\theta}{K_1} + \frac{\sin^2\theta}{K_2} & \sin\theta\cos\theta\left(\frac{1}{K_2} - \frac{1}{K_1}\right) \\ \sin\theta\cos\theta\left(\frac{1}{K_2} - \frac{1}{K_1}\right) & \frac{\sin^2\theta}{K_1} + \frac{\cos^2\theta}{K_2} \end{bmatrix} \tag{2}$$

where K_1 and K_2 are the permeabilities across and along filaments respectively, as shown in Fig. 3. To study the effect of mean bending of the canopy, we assume that the filaments are rotated as cantilevers with a constant θ, and solve Eq. 1 analytically. K_1 and K_2 are assumed to scale with the square of the distance between the filaments and are adjusted to account for the denser packing for non zero bending angles. The solution gives an expression for the wall-normal velocity at the interface between the canopy and the channel, which is used as a boundary condition for the overlying flow. This boundary condition links the transpiration velocity across the canopy/free flow interface with the pressure fluctuations above it, and takes the form

$$v' = -\beta p' \tag{3}$$
$$\beta = f(K_1, K_2, h_f, \alpha) \tag{4}$$

where α is the wavenumber of the perturbations.

Within the channel, we assume that the perturbations are inviscid and governed by Rayleigh's equation. An order of magnitude analysis shows that viscous terms are negligible in the channel, even when they are dominant within the substrate. Gomez-de

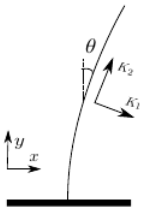

Figure 3: Permeability tensor after rotation of reference frame.

Segura *et al.* (2017) have performed a fully viscous analysis of the system and found the effect of viscosity to be limited to damping instabilities at small wavelengths, with no essential difference on the mechanisms or their modulation by the properties of the canopy. For the base velocity profile, an approximate turbulent profile is used (Cess, 1958) between the canopy tips. This follows from the assumption that the flow within the canopy is Stokesian and turbulence does not penetrate into the canopy. The resulting eigenvalue problem is solved using a Fourier spectral discretisation in x and a Chebyshev one in y.

Drag model

In this model the canopy is represented as a viscous drag force in the momentum equations. The assumption of a viscous drag can be considered valid for closely packed or dense canopies, within which the Reynolds number based on the local velocity and canopy spacing would be relatively low. This assumption also implies that, similar to the previous model, turbulence does not penetrate into the canopy. The governing equation then can be written as

$$\frac{\partial\vec{u}}{\partial t} + \vec{u}\nabla\vec{u} = -\frac{1}{\rho}\nabla P + \nu\nabla^2\vec{u} - \frac{1}{\rho}\mathbf{C}\vec{u} \tag{5}$$

where, $\mathbf{C}$ is the tensor of drag coefficients and is analogous to that given for $\mathbf{K^{-1}}$ in Eq. 2. The drag coefficients C_1 and C_2 are assumed constant inside the canopy. As the region including the canopy is resolved as part of the domain in the stability analysis, we derive a modified Rayleigh's equation

$$\begin{aligned}[(U\alpha - iC_{22})(D^2-\alpha^2) - \alpha(U'' + C'_{12}) \\ - (iC'_{11} + 2\alpha C_{12})D - i(C_{11} - C_{22})D^2]\tilde{v} = \sigma(D^2-\alpha^2)\tilde{v}\end{aligned} \tag{6}$$

where α is the streamwise wavelength of the perturbation, σ is the temporal growth rate, C_{ij} are the elements of $\mathbf{C}$, and D and the prime superscript indicate differentiation with respect to y. $\mathbf{C}$ is only non-zero within the canopy region.

For this case, a compact finite difference scheme is used to discretise the wall-normal direction, to avoid the excessive resolution that a Chebyshev discretisation would produce within the canopy. To obtain the base flow Eq. 5 is solved, assuming parallel flow, with a Cess turbulent viscosity between canopy tips and and neglecting advection within the canopy.

Model for dynamic clustering

The coherent bending of canopies also causes local clustering of the filaments. To model this, we consider a tall, dense canopy waving in response to flow over it. As the flow only penetrates into

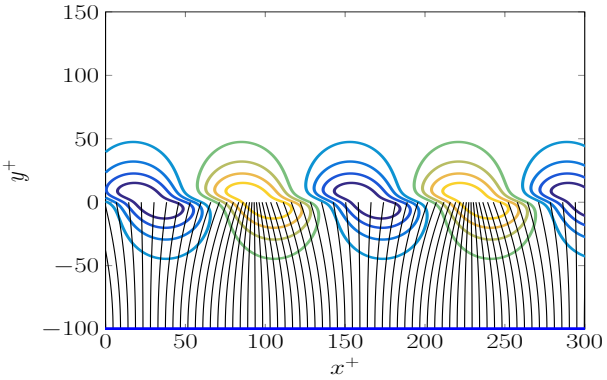

Figure 4: Clustering of canopy elements in response to the overlying Kelvin-Helmholtz-like instability. The contours show the perturbational streamlines obtained from the stability analysis, with shades of blue and yellow representing clockwise and counterclockwise rollers respectively.

a small region of the canopy, only its top portion is dynamically active. Even if the mean mean effect of canopy bending is small, as we will see bending would also have the effect of concentrating canopy tips in certain areas and vice versa. If we consider this effect while neglecting that of canopy inclination, we can model the canopy as if its elements merely slid from side to side in response to the velocity fluctuations. The displacement of the filaments is assumed to be proportional to the fluid forces on them, and therefore is modelled as proportional to the local velocity. Fig. 4 illustrates the relationship between filament deflection and clustering. In regions where the displacement increases along x, i.e. where consecutive canopy elements are increasingly displaced, the canopy would be sparser, and vice versa. If we linearise the dependence of the local drag coefficient on the canopy density we obtain

$$C_x = \bar{C}_x \left(1 - C_c \frac{\partial u}{\partial x}\right) \tag{7}$$

where u is the streamwise perturbational velocity, $\bar{C}_x$ is the average drag coefficient, and the constant C_c measures the sensitivity of C_x to clustering.

RESULTS

In agreement with prior studies, both the permeability and drag models reveal the formation of a Kelvin-Helmholtz-like instability at the canopy-fluid interface. In the drag model, this instability is a result of an inflected mean velocity profile, characteristic of canopy flows (Raupach *et al.*, 1996). In the porous substrate model, the instability is elicited by relaxation of the impermeability condition at the canopy-fluid interface (Jiménez *et al.*, 2001; García-Mayoral & Jiménez, 2011; Abderrahaman-Elena & Garcia-Mayoral, 2015), but both mechanisms are essentially the same.

Porous substrate model

The lengthscale of this instability is known to be set by the shear at the interface. Here, the lengthscale is set by the shape of the overlying turbulent mean velocity profile, which in turn scales in friction units calculated by defining u_τ at the canopy-fluid interface. This friction unit scaling can be observed in Fig. 6. In the case of stiff filaments, $\theta = 0$, $K_x = K_1$ and $K_y = K_2$, for which the solution of Brinkman's equation splits into two distinct branches for $K_1/K_2 > 1$ and $K_1/K_2 < 1$. Substrates lying in the former regime may find use in turbulent skin friction reduction and are discussed in Gomez-de Segura *et al.* (2017). In the case of interest for filament canopies, $K_1/K_2 < 1$, a single characterising parameter is observed to essentially govern the instability, as shown in Fig. 5:

$$\kappa_{Br}^+ = \sqrt{{K_1}^+ {K_2}^+} \tanh\left(\frac{h_f}{2y_c}\sqrt{\frac{K_1}{K_2}}\right) \tanh^2\left(\frac{h_f}{\sqrt{K_1}}\right) \tag{8}$$

where κ_{Br} is the empirically derived equivalent permeability, $y_c^+ \approx 8$ represents the height above the canopy where the vorticity of the base flow profile concentrates. This height has previously been found to set the length scale for the instability (García-Mayoral & Jiménez, 2011; Abderrahaman-Elena & Garcia-Mayoral, 2015). For deep canopies ($h_f >> \sqrt{K_x}$), and in the limit where the instabilities are fully developed, $\kappa_{Br} > 5$, the tanh terms are ≈ 1 and $\sqrt{K_x^+ K_y^+}$ is the dominant parameter driving the appearance of Kelvin-Helmholtz-like instabilities. This parameter was also obtained by Abderrahaman-Elena & Garcia-Mayoral (2015) using Darcy's equations to model the flow within the canopy. The similarity can be attributed to the large wall-normal permeabilities characteristic of canopies, which offer little resistance to flow penetrating into the canopy. As a result, the variation in the wall-normal direction of the perturbational pressure is low and the flow is qualitatively similar to that governed by Darcy's law.

The effect of mean bending of the filaments in the analysis is primarily reflected by the appearance of off-diagonal terms in the permeability tensor (Eq. 2). These terms are negligible for small filament bending angles, and it is shown in Fig. 7 that bending angles even up to 30 degrees have little effect on the instability characteristics. We will therefore neglect this effect in the following sections. It can also be observed in Fig. 5 that the maximum amplification of the instabilities asymptotes for high permeability values. This is a result of the boundary condition ($v' = -\beta p'$) used to model the porous medium in the analysis. At very high permeabilities, ($\beta \to \infty$) the pressure fluctuations tend to zero ($p' \to 0$). Physically, this can viewed as the mirroring of the overlying base velocity profile across the canopy interface. This resembles a free shear flow, providing the Kelvin-Helmholtz limit (Jiménez *et al.*, 2001; García-Mayoral & Jiménez, 2011). Once this limit is reached the amplification becomes independent of the value of permeability leading to the asymptotic regime.

Drag model

As in the previous model, the lengthscale of the instability is set by the shear at the canopy/free flow interface. By defining the friction velocity (u_τ) at this interface as the reference velocity, it is observed that the most amplified instabilities scale in friction units.

Comparing the variation of the amplification curves for the two models, as shown in Fig. 6, the high drag/low permeability region shows good agreement. However, we find a qualitative difference between the curves in the opposite limit of low drag/high permeability. As discussed in the previous section, the permeable substrate model exhibits an asymptotic limit of the amplification. In contrast, the drag model exhibits an optimum drag coefficient, for which the instability is most amplified. This optimum is the result of drag having two competing effects. The first is the effect on the mean profile - more drag implies more inflection in the profile, which enhances the instability. The second is the effect on the fluctuations - more drag implies smaller fluctuations and therefore weakens the instability. Both effects are balanced at the optimum value of the drag coefficient. This competition of effects is missed by the permeable

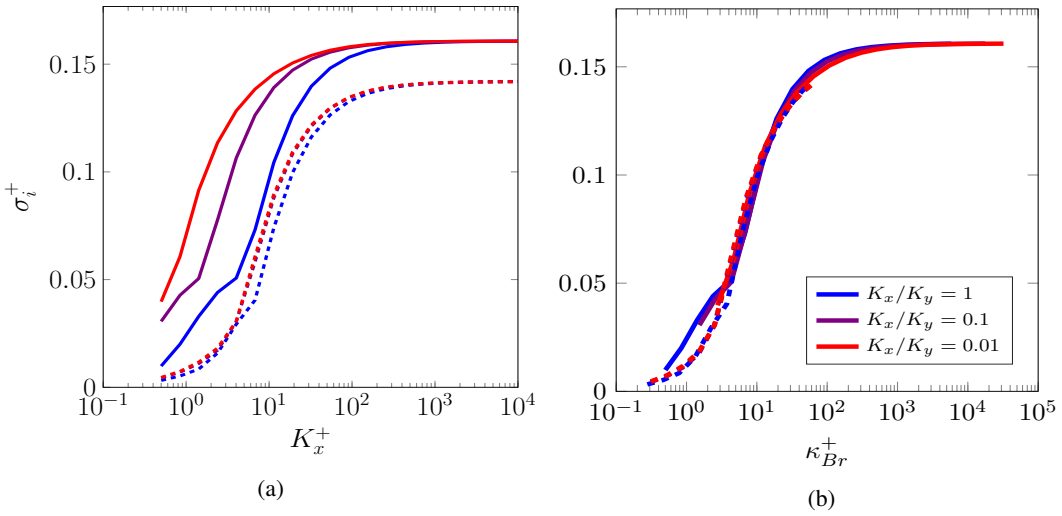

Figure 5: Variation in maximum amplification with (a) streamwise permeability and (b) equivalent permeability. Solid lines represent $h_f^+ = 100$, dashed lines- $h_f^+ = 10$.

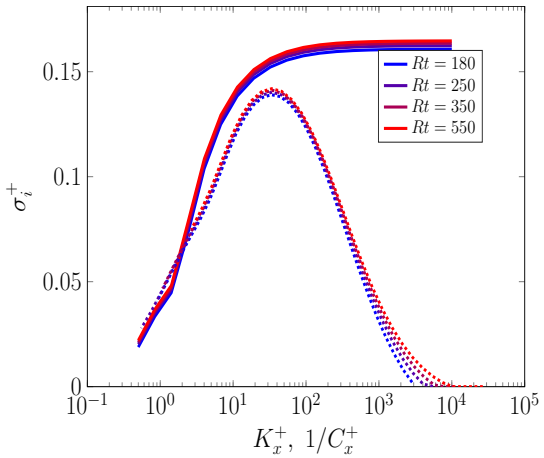

Figure 6: Maximum amplification vs. streamwise permeability/ inverse streamwise drag for varying Re_τ. Solid lines - porous substrate model, $h_f^+ = 10$, $K_x/K_y = 0.1$; dashed lines - drag model $h_f^+ = 18$, $C_y/C_x = 0.8$.

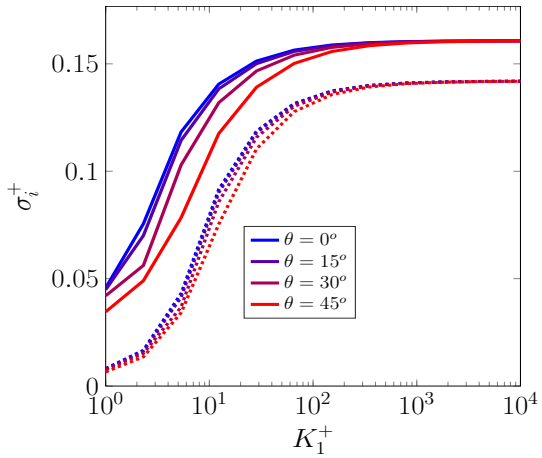

Figure 7: Maximum amplification vs. streamwise permeability for varying canopy bending angles. Solid lines represent $h_f^+ = 100$, dashed lines $h_f^+ = 10$. The anisotropy ratio, $K_1/K_2 = 10^{-1}$.

model, which does not require information on the shape of the base flow within the canopy.

Wall-normal drag was found to damp the most amplified modes, as can be observed in Fig. 8. This is due to the wall-normal drag obstructing the penetration of the Kelvin-Helmholtz like rollers into the canopy. The effect of mean canopy orientation was also studied using the drag model and the results corroborate those obtained with the permeable substrate model.

Dynamic clustering

The dynamic clustering of canopies has been modelled as the approximate response of the canopy elements to a sinusoidal velocity perturbation. Fig. 4 portrays the streamlines of the velocity perturbations over the approximate canopy response to them. These streamlines take the form of counter-rotating rollers, typical of the Kelvin-Helmholtz-like instability. The figure shows that the positions of the clockwise rollers, coincides with the regions of low filament density and are therefore less damped by the canopy drag. In turn, the counter-clockwise rollers coincide with regions of high drag. On increasing the intensity of clustering, that is for higher C_c in Eq. 7, this effect results in greater amplification of the instability, as is shown in Fig. 9, even though the magnitude of perturbational drag is locally increased. We examine only realisable values of C_c, i.e. those that do not produce negative drag coefficients locally. It is also worth noting that the maximum amplitude obtained in the limiting case of clustering, for which C_x locally reaches zero value, matches the values obtained for a case with zero pertubational drag. This case would correspond with some canopy regions being void of canopy elements. These preliminary results suggest that the canopy dynamics, particularly the spacial clustering of the canopy, can significantly affect the nature of the instability. However, this simplified model does not account for canopy inertia, and as a result, the canopy displacement is in phase with u. In a real canopy, it is possible that this phase relationship may vary according to the mechanical properties of the filaments.

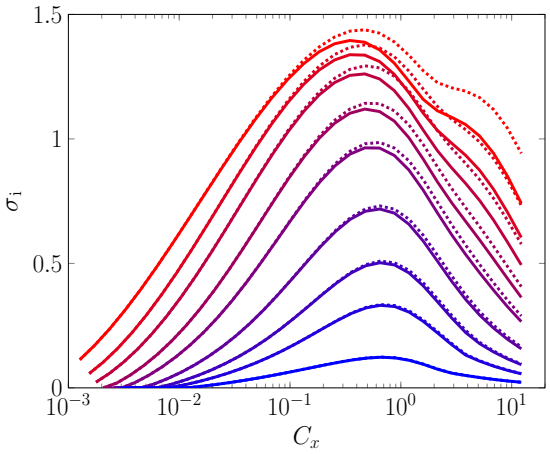

Figure 8: Variation of maximum amplification with the streamwise drag coefficient for varying filament heights. Solid lines show results for analysis with streamwise and wall-normal drag, dashed lines - streamwise drag only. $C_y/C_x = 0.8$, h_f^+ increases from blue to red.

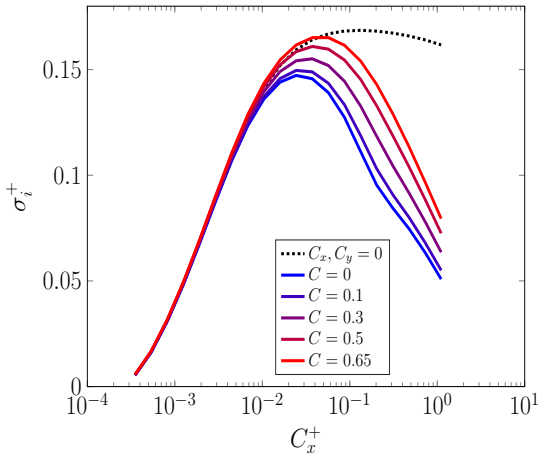

Figure 9: Change in maximum amplification for varying clustering intensities. Dashed lines shows limit obtained for analysis with no drag damping the perturbations.

CONCLUSIONS

The present study aims to relate the Kelvin-Helmholtz-like instabilities over filament canopies to the physical parameters of the canopy. Using a porous medium analogy, it is shown that the instability over dense canopies can be characterised using a single parameter $\kappa_{Br} \approx \sqrt{K_x^+ K_y^+}$ (Eq. 8). In designing synthetic canopies, this parameter can be used as a predictive metric to ascertain whether the instabilities triggered lie in the high amplification region or not. On comparing the results obtained using the two models we find that the drag model provides a more realistic representation of the low drag/high permeability regime. It also provides an optimum drag coefficient at which the most amplified instabilities are obtained. The models also show that the mean bending of the canopies does not affect the instability significantly, at least up to 30 degrees. However, the clustering of filaments due to dynamic bending is found to increase the amplification significantly due to positive feedback between the fluctuations in the streamwise velocity and in the drag coefficient.

REFERENCES

Abderrahaman-Elena, N. & Garcia-Mayoral, R. 2015 Preliminary analysis of turbulent coatings for turbulent drag reduction. In *Proceedings of TSFP9*.

Beavers, G. S. & Joseph, D. D. 1967 Boundary conditions at a naturally permeable wall. *Journal of fluid mechanics* **30** (01), 197–207.

Beneddine, S., Sipp, D., Arnault, A., Dandois, J. & Lesshafft, L. 2016 Conditions for validity of mean flow stability analysis. *Journal of Fluid Mechanics* **798**, 485–504.

Brinkman, H. C. 1949 A calculation of the viscous force exerted by a flowing fluid on a dense swarm of particles. *Applied Scientific Research* **1** (1), 27–34.

Cess, R. D. 1958 A survey of the literature on heat transfer in turbulent tube flow. Report 8-0529-R24. Westinghouse Research.

Dupont, S., Gosselin, F., Py, C., De Langre, E., Hemon, P. & Brunet, Y. 2010 Modelling waving crops using large-eddy simulation: comparison with experiments and a linear stability analysis. *Journal of Fluid Mechanics* **652**, 5–44.

Finnigan, J. J. 2000 Turbulence in plant canopies. *Annual Review of Fluid Mechanics* **32** (1), 519–571.

García-Mayoral, R. & Jiménez, J. 2011 Hydrodynamic stability and breakdown of the viscous regime over riblets. *Journal of Fluid Mechanics* **678**, 317–347.

Ghisalberti, M. & Nepf, H. 2009 Shallow flows over a permeable medium: The hydrodynamics of submerged aquatic canopies. *Transport in Porous Media* **78** (3 SPEC. ISS.), 385–402.

Inoue, E 1955 Studies of the phenomena of waving plants (honami) caused by wind. part 1: Mechanism and characteristics of waving plants phenomena. *J. Agric. Meteorol.(Japan)* **11**, 18–22.

Jiménez, J., Uhlmann, M., Pinelli, A. & Kawahara, G. 2001 Turbulent shear flow over active and passive porous surfaces. *Journal of Fluid Mechanics* **442**, 89–117.

Lacis, U. & Bagheri, S. 2017 A framework for computing effective boundary conditions at the interface between free fluid and a porous medium. *J. Fluid Mech.* **812**, 866–889.

Luminari, N., Airiau, C. & Bottaro, A. 2016 Drag-model sensitivity of kelvin-helmholtz waves in canopy flows. *Physics of Fluids* **28** (12), 124103.

Nepf, H. M. 2012 Flow and Transport in Regions with Aquatic Vegetation. *Annual Review of Fluid Mechanics* **44** (1), 123–142.

Ochoa-Tapia, J. A. & Whitaker, S. 1995 Momentum transfer at the boundary between a porous medium and a homogeneous fluidi. theoretical development. *International Journal of Heat and Mass Transfer* **38** (14), 2635–2646.

Py, C., de Langre, E. & Moulia, B 2006 A frequency lock-in mechanism in the interaction between wind and crop canopies. *Journal of Fluid Mechanics* **568**, 425.

Raupach, M. R., Finnigan, J. J. & Brunei, Y. 1996 Coherent eddies and turbulence in vegetation canopies: the mixing-layer analogy. *Boundary-Layer Meteorology* **78** (3-4), 351–382.

Gomez-de Segura, G., Sharma, A. & Garcia-Mayoral, R. 2017 Turbulent drag reduction over anisotropic porous coatings. In *Proceedings of TSFP10*.

Singh, R., Bandi, M. M., Mahadevan, A. & Mandre, S. 2016 Linear stability analysis for monami in a submerged seagrass bed. *Journal of Fluid Mechanics* **786**, R1.

White, B. L. & Nepf, H. M. 2007 Shear instability and coherent structures in shallow flow adjacent to a porous layer. *Journal of Fluid Mechanics* **593**, 1–32.

Zampogna, G. A. & Bottaro, A. 2016 Fluid flow over and through a regular bundle of rigid fibres. *J. Fluid Mech.* **792**, 5–35.

Zampogna, G A, Pluvinage, F, Kourta, A & Bottaro, A 2016 Instability of canopy flows. *Water Resources Research* **52** (7), 5421–

5432.